

ImmunoSPECT and ImmunoPET of IGF-1R Expression with the Radiolabeled Antibody R1507 in a Triple-Negative Breast Cancer Model

Sandra Heskamp¹, Hanneke W.M. van Laarhoven¹, Janneke D.M. Molkenboer-Kuennen², Gerben M. Franssen², Yvonne M.H. Versleijen-Jonkers¹, Wim J.G. Oyen², Winette T.A. van der Graaf¹, and Otto C. Boerman²

¹Department of Medical Oncology, Radboud University Nijmegen Medical Centre, Nijmegen, The Netherlands; and ²Department of Nuclear Medicine, Radboud University Nijmegen Medical Centre, Nijmegen, The Netherlands

The insulinlike growth factor 1 receptor (IGF-1R) is a new target for the treatment of breast cancer. Patients with breast cancer lesions that express IGF-1R may benefit from treatment with anti-IGF-1R antibodies. Therefore, the aim of the present study was to develop a noninvasive, in vivo imaging method, using radiolabeled antibodies, to visualize IGF-1R expression. **Methods:** R1507 is a monoclonal antibody directed against the IGF-1R. In vitro, the affinity and internalization kinetics of ¹¹¹In-R1507 were determined using the IGF-1R-expressing triple-negative breast cancer cell line SUM149. In vivo, the pharmacodynamics of ¹¹¹In-R1507 and ¹²⁵I-R1507 were determined in mice with subcutaneous SUM149 tumors. ¹¹¹In-R1507 SPECT and ⁸⁹Zr-R1507 PET images of mice with subcutaneous SUM149 tumors were acquired at 1, 3, and 7 d after injection. **Results:** ¹¹¹In-R1507 (concentration required to inhibit binding by 50%, 0.1 nM) was slowly internalized by SUM149 cells. ¹¹¹In-R1507 specifically and efficiently accumulated in the SUM149 xenografts: the tumor uptake was 20 percentage injected dose per gram (%ID/g), 33 %ID/g, and 31 %ID/g at 1, 3, and 7 d after injection, respectively. ¹²⁵I-R1507 accumulated in the tumor less efficiently. Small-animal SPECT and small-animal PET of mice clearly visualized the subcutaneous SUM149 xenograft, with increasing contrast at later time points. **Conclusion:** ¹¹¹In-R1507 and ⁸⁹Zr-R1507 are new tracers to noninvasively determine IGF-1R expression in vivo in breast cancer xenografts using SPECT and PET. In the future, these techniques may enable patient selection for IGF-1R-targeted therapy.

Key Words: IGF-1R; PET; SPECT; antibody; breast cancer

J Nucl Med 2010; 51:1565–1572

DOI: 10.2967/jnumed.110.075648

Triple-negative breast tumors are estrogen receptor-, progesterone receptor-, and *HER2/neu*-negative. Although they account for only 10%–17% of all breast carcinomas (1–8), tumors are often high grade and patients are rela-

tively young and have a reduced breast cancer-specific survival, compared with patients with estrogen receptor- or *HER2/neu*-expressing tumors (2,9). Because targeted treatments are currently not approved for patients with triple-negative breast cancer, the standard systemic treatment is chemotherapy. However, several new targeted agents are currently being tested in clinical trials for their efficacy in patients with triple-negative breast cancer (10).

A potential new target for the treatment of triple-negative breast cancer is the insulinlike growth factor 1 receptor (IGF-1R). The IGF-1R is a transmembrane receptor expressed in many human cancers, including 36% of all triple-negative breast carcinomas (11). It plays a role in proliferation, apoptosis, angiogenesis, and tumor invasion (12–14), and its expression may be related to resistance to cytotoxic-, anti-estrogen-, and *HER2/neu*-targeted therapy (15–18). On binding of insulinlike growth factors to the receptor, adaptor proteins, such as insulin-receptor substrate-1 (IRS-1) and IRS-2, are recruited to the phosphorylation site of the cytoplasmic domain (19–21). Subsequently, the phosphatidylinositol-3-kinase and mitogen-activated protein kinase pathways can be activated, resulting in proliferation and inhibition of apoptosis (13,14).

Currently, several small-molecule inhibitors and antibodies directed against the IGF-1R are being developed and tested in phase I and II clinical trials. Preliminary results of these studies have shown the safety and tolerability of targeting the IGF-1R. Stable disease and objective responses have been reported in patients treated with these new agents, but no relationship with the IGF-1R expression has been tested in a structured way (22).

In vitro studies have shown that IGF-1R expression is necessary for antitumor activity of anti-IGF-1R antibodies (23,24). Therefore, patient selection for IGF-1R-targeted therapy may be based on receptor expression. Thus far, studies on IGF-1R expression have been performed mainly on tumor tissue sections using immunohistochemistry. However, this technique cannot be used to measure the expression in different tumor lesions and different regions within a tumor, because this would require multiple invasive procedures. Furthermore, the expression of IGF-1R may change

Received Feb. 1, 2010; revision accepted Jul. 8, 2010.

For correspondence or reprints contact: Sandra Heskamp, Department of Nuclear Medicine, Radboud University Nijmegen Medical Centre, Internal Postal Code 444, P.O. Box 9101, 6500 HB Nijmegen, The Netherlands.

E-mail: s.heskamp@nucmed.umcn.nl

COPYRIGHT © 2010 by the Society of Nuclear Medicine, Inc.

in the course of time (e.g., because of tumor growth and therapy). Therefore, the aim of the present study was to develop a noninvasive imaging method that allows monitoring of the membranous IGF-1R expression in all breast cancer lesions during the course of the disease. For this purpose, the fully human anti-IGF-1R monoclonal antibody R1507, directed against the human IGF-1R, was radiolabeled with ^{111}In or ^{89}Zr for in vivo imaging of IGF-1R expression with immunoSPECT and immunoPET, respectively.

MATERIALS AND METHODS

Cell Culture

The triple-negative breast cancer cell line SUM149 (Asterand) was cultured and maintained as monolayer in culture flasks in Ham's F12 medium (GIBCO; BRL Life Sciences Technologies) supplemented with 5% fetal calf serum, 10 mM *N*-(2-hydroxyethyl)piperazine-*N'*-(2-ethanesulfonic acid) (HEPES), hydrocortisone (1 $\mu\text{g}/\text{mL}$), and insulin (5 $\mu\text{g}/\text{mL}$) at 37°C in a humidified atmosphere with 5% CO_2 . MCF-7 cells were cultured in RPMI 1640 medium (GIBCO; BRL Life Sciences Technologies), supplemented with 10% fetal calf serum, 2 mM glutamine, penicillin (100 units/mL), and streptomycin (100 $\mu\text{g}/\text{mL}$).

Radiolabeling

Radiolabeling of R1507 with ^{111}In . The fully human monoclonal antibody R1507 was obtained from Roche Diagnostics and is directed against an epitope on the extracellular domain of the human IGF-1R. R1507 was conjugated with isothiocyanatobenzyl-diethylenetriaminepentaacetic acid (ITC-DTPA) (Macrocyclus) in 0.1 M NaHCO_3 , pH 9.5, using a 10-fold molar excess of ITC-DTPA for 1 h at room temperature (RT). The unbound ITC-DTPA was removed from the reaction mixture by dialysis against 0.25 M ammonium acetate buffer, pH 5.4. DTPA-R1507 (10 μg) was incubated with 3.7 MBq of ^{111}In (Covidien BV) in 0.1 M 2-(*N*-morpholino)ethanesulfonic acid buffer, pH 5.4, at RT, under strict metal-free conditions for 30 min. For SPECT, 22 μg of DTPA-R1507 was incubated with 244 MBq of ^{111}In . Labeling efficiency was determined using instant thin-layer chromatography (ITLC) on TEC Control chromatography strips (Biodex), with 0.1 M citrate buffer, pH 6.0, as the mobile phase. If labeling efficiency was below 95%, the reaction mixture was purified on a PD-10 column (Amersham Biosciences), eluted with phosphate-buffered saline, containing 0.5% bovine serum albumin (BSA). Radiochemical purity of ^{111}In -DTPA-R1507 (^{111}In -R1507) exceeded 98% in all experiments.

Radiiodination of R1507. R1507 (40 μg) was iodinated with 18.5 MBq of ^{125}I (Amersham) in an IODO-GEN-coated (Pierce) vial, in 0.5 M phosphate buffer, pH 7.2, at RT for 15 min. Labeling efficiency as determined by ITLC was 92.0%. The reaction mixture was purified on a PD-10 column eluted with phosphate-buffered saline containing 0.5% BSA. Radiochemical purity of ^{125}I -R1507 exceeded 99%.

Radiolabeling of R1507 with ^{89}Zr . R1507 was modified with succinyl-desferal-iron-tetrafluorophenol (VU University Medical Center) ester as described previously (25). In short, a 2-fold molar excess of succinyl-desferal-iron-tetrafluorophenol was incubated with R1507 for 30 min at RT in 0.1 M Na_2CO_3 , pH 9.5. Subsequently, the sample was incubated with ethylenediaminetetraacetic acid (final concentration, 1.5 mg/mL) at pH 4.3 for 30 min at 35°C to remove the iron from the chelate. The reaction mixture was

purified on a PD-10 column, eluted with 5 mg of gentisic acid per milliliter. The R1507 conjugate (0.5 mg) was radiolabeled with 500 MBq of ^{89}Zr (IBA Pharma) in 0.5 M HEPES, pH 7.2, for 90 min at 35°C. Labeling efficiency as determined by ITLC was 54%. The reaction mixture was purified on a PD-10 column eluted with 5 mg of gentisic acid per milliliter. The radiochemical purity of ^{89}Zr -*N*-succinyl-desferal-R1507 (^{89}Zr -R1507) was 98%.

In Vitro Characteristics of ^{111}In -DTPA-R1507

Immunoreactive Fraction. The immunoreactive fractions of ^{111}In -R1507, ^{125}I -R1507, and ^{89}Zr -R1507 were determined as described by Lindmo et al. (26). A serial dilution of MCF-7 cells (4.8×10^6 to 30×10^6 cells/mL) in RPMI 0.5% BSA was incubated with 200 Bq of ^{111}In -R1507, ^{125}I -R1507, or ^{89}Zr -R1507. Nonspecific binding was determined by adding an excess of unlabeled R1507 (67 nM) to a duplicate of the lowest cell concentration. After 1 h of incubation at 37°C, cells were centrifuged, and the activity in the cell pellet was measured in a shielded 7.62-cm (3-in) well-type γ -counter (Perkin-Elmer). The inverse of the specific cell-bound activity was plotted against the inverse of the cell concentration, and the immunoreactive fraction was calculated from the y -axis intercept.

Internalization. SUM149 cells were cultured in 6-well plates and were incubated with 1.9 kBq of ^{111}In -R1507 (specific activity, 0.3 MBq/ μg) for 1, 2, 4, 8, 24, and 48 h, in 2 mL of binding buffer (Ham's F12, 10 mM HEPES, 0.5% BSA) at 37°C in a humidified atmosphere with 5% CO_2 . Nonspecific binding and internalization were determined by coincubation with 67 nM unlabeled R1507. After incubation, acid wash buffer (0.1 M HAc, 0.15 M NaCl, pH 2.6) was added for 10 min to remove the membrane-bound fraction of the cell-associated ^{111}In -R1507. Subsequently, cells were harvested from the 6-well plates using cotton plugs, and the amount of membrane-bound and internalized activity was measured in a γ -counter.

Affinity. SUM149 cells were cultured to confluency in 6-well plates. To determine the concentration required to inhibit binding by 50% (IC_{50}), cells were incubated for 4 h at 4°C in 2 mL of binding buffer with 1.9 kBq of ^{111}In -R1507 (specific activity, 0.3 MBq/ μg) and increasing concentrations of unlabeled R1507 (10^{-2} to 10^3 pM). After incubation and washing, cell-associated activity was measured in a γ -counter.

Immunohistochemistry of SUM149 Tumors

IGF-1R expression on SUM149 xenografts was analyzed by immunohistochemistry. SUM149 tumors were fixed in 4% formalin and embedded in paraffin. Tumor sections (4 μm) were deparaffinized in xylol for 15 min and rehydrated in graded dilutions of ethanol in water. Antigens were retrieved using 10 mM sodium citrate, pH 6.0, for 10 min at 100°C. Endogenous peroxidase activity was blocked with 3% H_2O_2 in phosphate-buffered saline (10 min at RT), and nonspecific binding was blocked by incubation with normal goat serum (30 min at RT). Subsequently, tumor sections were incubated with 0.6 μg of polyclonal rabbit anti-IGF-1R β antibody per milliliter (Cell Signaling Technology) overnight at 4°C, followed by incubation with a goat-antirabbit biotinylated secondary antibody (Vector Laboratories) for 30 min at 37°C. Finally, avidin-biotin-enzyme complex (Vector Laboratories) was applied for 30 min at 37°C and 3,3'-diaminobenzidine was used to develop the tumor sections.

Animal Studies

Animal experiments were performed in female BALB/c nude mice and were conducted in accordance with the principles laid

out by the revised Dutch Act on Animal Experimentation (1997) and approved by the institutional Animal Welfare Committee of the Radboud University Nijmegen. Mice (6–8 wk old) were inoculated subcutaneously with 5×10^6 SUM149 cells (mixed 2:1 with Matrigel; BD Biosciences). Experiments started when the tumors reached approximately 0.1 cm^3 .

Protein Dose-Escalation Study of ^{111}In -R1507. Seven groups ($n = 6$) of mice with subcutaneous SUM149 xenografts received an intravenous injection of 0.2 MBq of ^{111}In -R1507 (specific activity, $0.4 \text{ MBq}/\mu\text{g}$) in the tail. To study the effect of the antibody protein dose on the biodistribution of ^{111}In -R1507, the groups received increasing protein doses of R1507 (1–1,000 μg). Three days after injection, mice were euthanized using O_2 - CO_2 asphyxiation. The uptake of ^{111}In -R1507 was measured in the tumor, blood, muscle, lung, liver, kidney, spleen, small intestine, pancreas, and salivary gland as described previously (27).

Pharmacodynamics of Radiolabeled R1507. Three groups of mice ($n = 12$) with subcutaneous SUM149 xenografts received an intravenous injection of 0.4 MBq of ^{111}In -R1507 (specific activity, $0.8 \text{ MBq}/\mu\text{g}$) and 0.2 MBq of ^{125}I -R1507 (specific activity, $0.4 \text{ MBq}/\mu\text{g}$). To determine the IGF-1R-mediated uptake of the radiolabeled R1507, 6 mice per group received an excess of unlabeled R1507 (500 μg) to block the IGF-1R *in vivo*. One, 3, and 7 d after injection of radiolabeled R1507, mice were euthanized, and uptake of radiolabeled R1507 was determined as described for the dose-escalation study.

ImmunoSPECT with ^{111}In -R1507. Five BALB/c mice bearing SUM149 xenografts received an intravenous injection of 17.2 MBq of ^{111}In -R1507 (specific activity, $10.9 \text{ MBq}/\mu\text{g}$). One mouse received an excess of unlabeled R1507 (1,000 μg) to determine the nonspecific uptake of R1507. Immediately after injection and at 1, 3, and 7 d after injection, images were acquired with the U-SPECT-II (MILabs) (28). Mice were scanned under general anesthesia (isoflurane and O_2) for 30–120 min using the 1.0-mm-diameter pinhole rat collimator tube. At day 7, the mice were euthanized, and the uptake of ^{111}In -R1507 in dissected tissue was determined as described for the dose-escalation study. Scans were reconstructed with software from MILabs, which uses an ordered-subset expectation maximization algorithm, with a voxel size of 0.375 mm. Representative cross-sections located approximately in the center of the tumor were displayed. Tumor-to-liver ratios were calculated with the Inveon Research Workplace software (version 2.2; Siemens Preclinical Solutions).

ImmunoPET with ^{89}Zr -R1507. Six BALB/c mice bearing SUM149 xenografts received an intravenous injection of 5.3 MBq of ^{89}Zr -R1507 (specific activity, $0.53 \text{ MBq}/\mu\text{g}$). Immediately after injection and at 1, 3, and 7 d after injection, PET images were acquired for 3 mice with the Inveon animal PET scanner (29) (Siemens Preclinical Solutions) under general anesthesia (isoflurane- O_2) for 10–30 min. At day 7, all mice were euthanized, and the uptake of ^{89}Zr -R1507 was determined *ex vivo* as described for the dose-escalation study. Scans were reconstructed using Inveon Acquisition Workplace software (version 1.2) using an ordered-set expectation maximization 3-dimensional maximum a posteriori algorithm with the following parameters: matrix, $256 \times 256 \times 159$; pixel size, $0.43 \times 0.43 \times 0.8 \text{ mm}$; and a uniform-variance maximum a posteriori prior, 0.05 mm. Representative cross-sections located approximately in the center of the tumor were displayed. Tumor-to-liver ratios were calculated with the Inveon Research Workplace software (version 2.2).

Statistical Analysis

Statistical analyses were performed using SPSS software (version 16.0; SPSS, Inc.) and Prism (version 4.00; GraphPad Software) for Windows (Microsoft). Differences in uptake of radiolabeled R1507 were tested for significance using the non-parametric Mann-Whitney test. A P value below 0.05 was considered significant.

RESULTS

In Vitro Characteristics of R1507

The Lindmo assay showed that the immunoreactive fractions of ^{111}In -R1507, ^{125}I -R1507, and ^{89}Zr -R1507 were, respectively, 99%, 88%, and 87%. ^{111}In -R1507 was slowly internalized by SUM149 cells (Fig. 1). During the first hours of incubation, ^{111}In -R1507 was mainly membrane-bound. The internalized fraction gradually increased until 62% of the cell-associated activity was internalized after 48 h of incubation. A typical binding plot of the IC_{50} analysis is shown in Figure 2. R1507 exhibited an IC_{50} value of 0.1 nM (95% confidence interval, 0.08–0.12 nM) for the IGF-1R on SUM149 cells.

Immunohistochemistry of SUM149 Tumors

Immunohistochemistry on tumor sections of SUM149 xenografts revealed both cytoplasmic and membranous IGF-1R expression (Fig. 3).

Dose-Escalation Study

A dose-escalation study was performed with ^{111}In -R1507 to determine the optimal protein dose of R1507 for *in vivo* imaging. Mean tumor weight at dissection was $112 \pm 45 \text{ mg}$. ^{111}In -R1507 showed high specific uptake in SUM149 xenografts on day 3 at doses less than 10 μg of antibody per mouse (Fig. 4). The highest uptake in the tumor was found

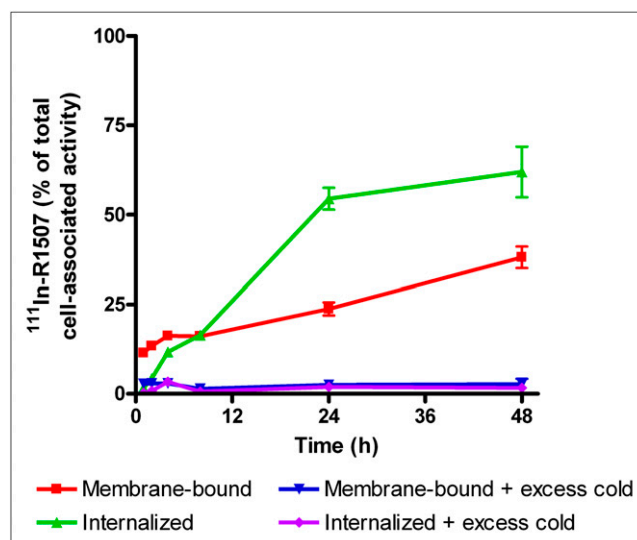


FIGURE 1. Internalization kinetics of ^{111}In -R1507 in SUM149 cells. Binding and internalization are presented as percentage of total cell-associated activity after 48 h of incubation (mean \pm SD).

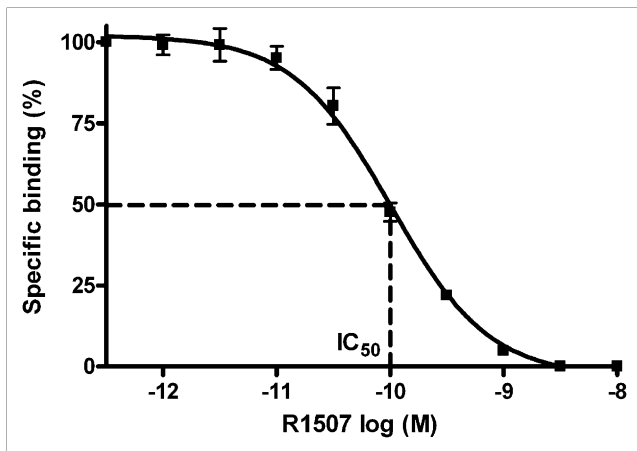


FIGURE 2. Typical binding plot of ^{111}In -R1507 and SUM149 cells. Binding is presented as mean \pm SD. R1507 exhibited an IC_{50} value of 0.1 nM.

at antibody protein doses of 3 μg or less (1 μg , 38 ± 11 percentage injected dose per gram [%ID/g]; 3 μg , 35 ± 6 %ID/g). Tumor uptake was significantly lower at an antibody protein dose of 10 μg (15 ± 4 %ID/g, $P = 0.002$). At a dose of 300 μg , the tumor uptake further decreased to 9 ± 1 %ID/g ($P = 0.004$). The highest tumor-to-blood ratios were obtained at a protein dose of 1 (2.7 ± 1.1) and 3 (2.4 ± 0.5) μg of R1507. The SUM149 tumor was the only tissue showing specific uptake of R1507, as evidenced by the reduced uptake at antibody doses above 100 μg .

Pharmacodynamics of Radiolabeled R1507

Results of the pharmacodynamics study are summarized in Figure 5. Mean tumor weight at dissection was 142 ± 66 mg. At all time points, ^{111}In -R1507 showed significantly higher tumor uptake than ^{125}I -R1507 ($P < 0.05$). One, 3, and 7 d after injection, the tumor uptake of ^{111}In -R1507 was, respectively, 20 ± 6 %ID/g, 33 ± 6 %ID/g, and 31 ± 4 %ID/g, compared with 8 ± 1 %ID/g, 7 ± 1 %ID/g, and 5 ± 1 %ID/g for ^{125}I -R1507. The tumor-to-blood ratio of ^{111}In -R1507 was the highest at 7 d after injection (3.8 ± 0.3) and for ^{125}I -R1507 3 d after injection (0.7 ± 0.1). Highest tumor-to-liver ratios of ^{111}In -R1507 and ^{125}I -R1507 were also obtained at day 7 (11.8 ± 1.7) and day 3 (3.3 ± 0.6), respectively. The tumor was the only tissue showing IGF-1R-mediated uptake of ^{111}In -R1507, as evidenced by the markedly reduced tumor uptake in the mice that received an excess of unlabeled R1507 (5.6 %ID/g at day 7). Uptake in the other organs was not affected by an excess of unlabeled R1507.

ImmunoSPECT with ^{111}In -R1507

One day after injection, the subcutaneous SUM149 tumor was clearly visualized on the SPECT images (Fig. 6). At later time points, the tumor-to-background contrast improved further because of clearance of ^{111}In -R1507 from the blood. SPECT images also showed uptake of ^{111}In -R1507 in the liver, spleen, and salivary glands. Tumor-to-

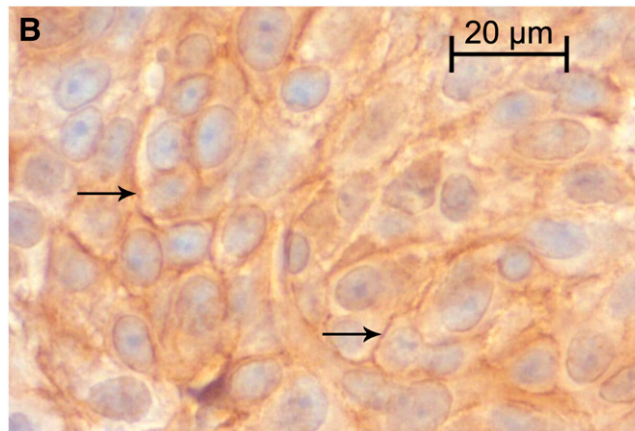
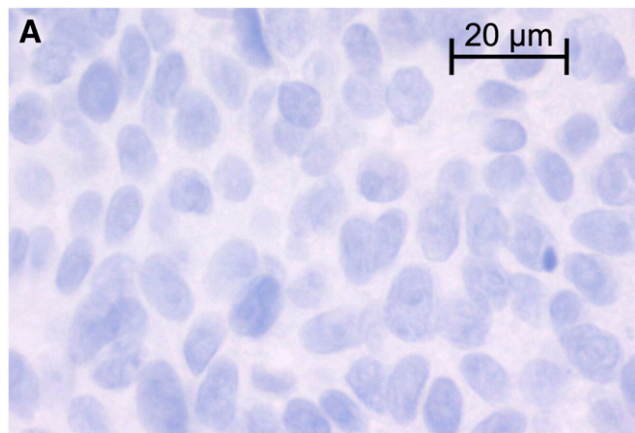


FIGURE 3. Typical example of immunohistochemical analysis of IGF-1R expression of an SUM149 tumor (tumor size, 0.5 cm^3). (A) Negative control. (B) Membranous and cytoplasmic IGF-1R staining. Arrows indicate membrane staining.

liver ratios were calculated from the SPECT images at 1, 3, and 7 d after injection and were 1.9 ± 0.6 , 3.5 ± 1.2 , and 5.8 ± 1.8 , respectively. The ex vivo biodistribution, at 7 d after injection, revealed that the mean tumor uptake of ^{111}In -R1507 was 20.9 ± 2.4 %ID/g (Table 1). Mean tumor weight at dissection was 150 ± 60 mg. The tumor-to-blood ratio was 3.8 ± 0.7 , and the tumor-to-liver ratio was 7.5 ± 1.2 . The SUM149 tumor of the mouse that received an excess of unlabeled R1507 could hardly be visualized by SPECT (Fig. 6D). The tumor uptake of ^{111}In -R1507 was only 4%, and the tumor-to-blood and tumor-to-liver ratios were 0.8 and 1.5, respectively.

ImmunoPET with ^{89}Zr -R1507

One day after injection of ^{89}Zr -R1507, SUM149 xenografts were clearly visualized with small-animal PET (Fig. 7). From day 1 to day 7, tumor-to-background contrast increased because of the clearance of ^{89}Zr -R1507 from the blood and background tissues. Tumor-to-liver ratios were calculated from the PET images and increased over time. At days 1, 3, and 7, tumor-to-liver ratios were 1.9 ± 0.1 , 2.9 ± 0.3 , and 4.7 ± 0.3 , respectively. The ex vivo

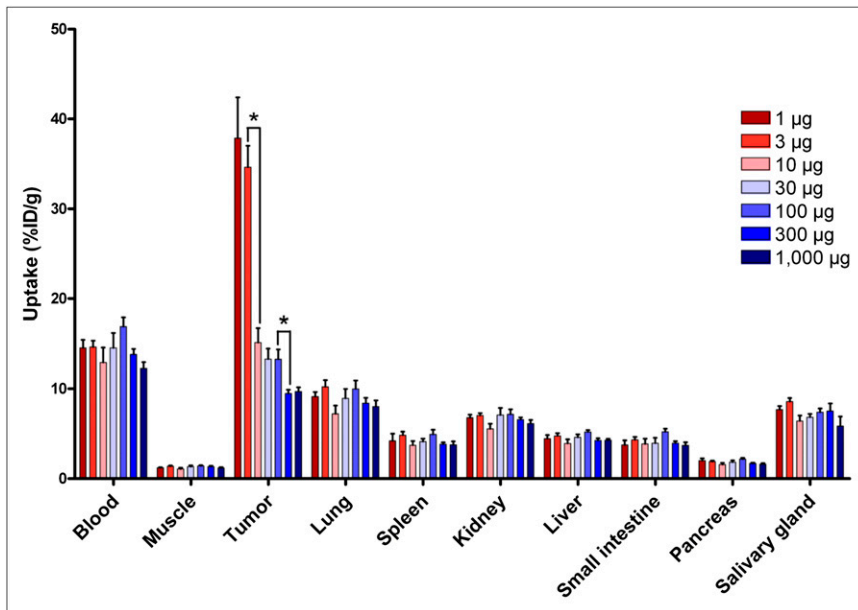


FIGURE 4. Dose-escalation study of ^{111}In -R1507 in mice with subcutaneous SUM149 xenografts, 3 d after injection. Values are presented as mean %ID/g of tissue \pm SD for 5 mice per group ($*P < 0.05$).

biodistribution study, at 7 d after injection, showed that the mean tumor uptake was 22 ± 3 %ID/g (Table 1). Mean tumor weight at dissection was 347 ± 70 mg. The tumor-to-blood and tumor-to-liver ratios were 3.9 ± 0.5 and 4.8 ± 0.2 , respectively. Besides tumor uptake, PET images also revealed nonspecific liver, spleen, salivary gland, and bone uptake.

DISCUSSION

The present study showed that both ^{111}In -R1507 and ^{89}Zr -R1507 efficiently accumulated in IGF-1R-expressing SUM149 tumors and were excellent tracers for noninvasive imaging of IGF-1R expression with immunoSPECT and immunoPET. In vitro experiments showed that R1507 has favorable characteristics for in vivo imaging. The immunoreactivity of the R1507 antibody was retained after the labeling procedure. Furthermore, R1507 is an internalizing antibody with high affinity for the IGF-1R (IC_{50} , 0.1 nM). The results of the comparative biodistribution study with ^{111}In -R1507 and ^{125}I -R1507 revealed higher tumor uptake of ^{111}In -R1507 than of ^{125}I -R1507, at all time points. Because R1507 is an internalizing antibody, residualizing radionuclides such as ^{111}In result in higher tumor retention

than does the nonresidualizing radionuclide ^{125}I (30,31). Therefore, we selected ^{111}In -R1507 and ^{89}Zr -R1507 for immunoSPECT and immunoPET of IGF-1R expression. The dose-escalation study showed that ^{111}In -R1507 efficiently targeted SUM149 xenografts at antibody protein doses up to 3 μg . At higher doses the tumor uptake decreased, presumably due to saturation of the IGF-1R.

Both ^{111}In -R1507 SPECT and ^{89}Zr -R1507 PET clearly visualized the IGF-1R-expressing breast cancer xenografts, with increasing contrast at later time points. Although R1507 does not cross-react with the murine IGF-1R, SPECT and PET images also revealed uptake in the liver, spleen, and salivary glands. The dose-escalation study showed that this uptake was not IGF-1R-mediated. The biodistributions of ^{89}Zr -R1507 and ^{111}In -R1507 were comparable, except for uptake in the bone. PET images clearly revealed bone uptake of ^{89}Zr -R1507, whereas bone uptake was not observed in the ^{111}In -R1507 SPECT images. Differences in bone uptake between ^{89}Zr -labeled antibodies and other residualizing radionuclides have been described previously for internalizing antibodies. Dijkers et al. showed that bone uptake of ^{89}Zr -labeled trastuzumab was significantly higher than that of ^{111}In -labeled trastuzumab

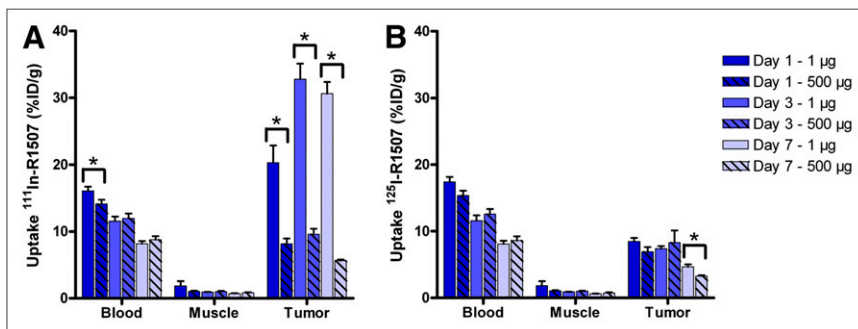
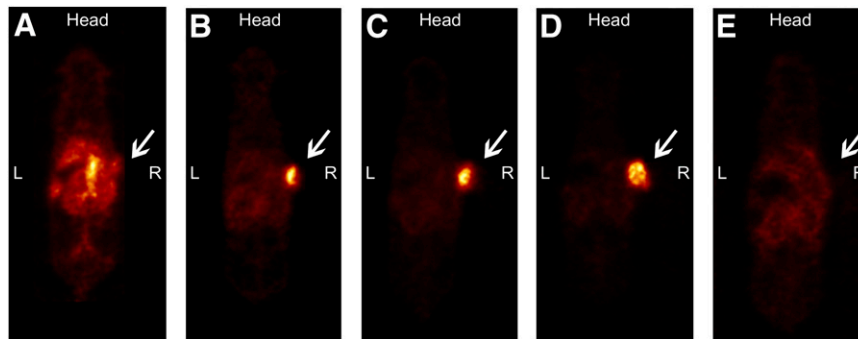


FIGURE 5. Biodistribution of ^{111}In -R1507 (A) and ^{125}I -R1507 (B) at 1, 3, and 7 d after injection in mice with subcutaneous SUM149 tumors. Values are presented as mean %ID/g of tissue \pm SD for 5 mice per group ($*P < 0.05$).

FIGURE 6. SPECT images of mouse with subcutaneous SUM149 tumor immediately after injection (A) and at 1 (B), 3 (C), and 7 (D) d after injection of 17.2 MBq of ^{111}In -R1507 (1.6 μg). Tumor-to-liver ratios in this mouse, calculated from SPECT images, were 1.5, 3.3, and 5.6 at 1, 3, and 7 d after injection, respectively. Ex vivo biodistribution study on day 7 revealed that tumor uptake of ^{111}In -R1507 for this mouse was 23 %ID/g. (E) SPECT image of mouse with subcutaneous SUM149 tumor at 7 d after injection of 17.2 MBq of ^{111}In -R1507 and excess of unlabeled R1507 (1,000 μg). Tumor-to-liver ratios in this mouse, calculated from SPECT images, were 1.1, 1.3, and 1.5 at 1, 3, and 7 d after injection, respectively. Ex vivo biodistribution on day 7 revealed that tumor uptake of ^{111}In -R1507 was 4.0 %ID/g. SUM149 tumors are indicated by arrows.



(32). Furthermore, Perk et al. reported an increased bone uptake of ^{89}Zr -cetuximab, compared with ^{88}Y - and ^{177}Lu -labeled cetuximab (33). These data indicate that ^{89}Zr might be incorporated in the bone more efficiently than other radiometals.

Previous in vitro studies have shown that IGF-1R expression strongly correlates with response to anti-IGF-1R antibodies (23,24). Therefore, IGF-1R expression on tumor lesions may be a suitable criterion to select patients for IGF-1R-targeted therapy. However, high IGF-1R expression alone was not sufficient to respond to anti-IGF-1R treatment (23,24). Other components in the IGF-1R pathway may also have a predictive value for response. Zha et al. showed that the adaptor proteins IRS-1 and IRS-2 and the ligand IGF-2 have predictive value for response to anti-IGF-1R antibodies (23). Other studies have also shown that IGF-1R, IRS-1, IGF-1, and IGF-2 expression correlates with sensitivity to IGF-1R tyrosine kinase inhibitors (34,35). The subcellular location of IGF-1R expression may also influence whether patients will respond to anti-IGF-1R antibodies. Previous studies have focused on total IGF-1R expression (membranous and cytoplasmic) or messenger RNA expression (23,24,34,35), whereas antibodies will target only IGF-1R expressed on the cell membrane. Therefore, membranous IGF-1R expression may be a better predictor of response than is total IGF-1R expression, if and when the downstream pathway lacks escape mechanisms.

Membranous IGF-1R expression can be determined on tumor sections using immunohistochemistry. Evaluation of IGF-1R expression is usually performed on archival tumor material because a new biopsy would require an invasive procedure. IGF-1R expression may change over time because of cytotoxic, antiestrogen, or anti-HER2 treatment or tumor progression (15–18). Noninvasive imaging of membranous IGF-1R expression would allow monitoring of the expression of all tumor lesions at several time points. Our studies showed that both ^{111}In -R1507 SPECT and ^{89}Zr -R1507 PET are excellent methods to visualize membranous IGF-1R expression in breast cancer xenografts. However,

these experiments were performed under optimal conditions, because R1507 does not cross-react with the murine IGF-1R. In patients, radiolabeled R1507 will also recognize the IGF-1R, which is widely expressed in normal tissues. This could result in enhanced uptake in IGF-1R-expressing normal tissues, including muscle, cartilage, and bone (36–38). Future studies will have to show whether imaging of IGF-1R expression with SPECT or PET is also feasible in patients.

Other approaches, besides using radiolabeled antibodies, for in vivo imaging of the IGF-1R expression have already been studied. Cornelissen et al. (39) have used ^{111}In -IGF-1 (E3R), an analog of IGF-1 that does not bind IGFBPs, to visualize IGF-1R expression of subcutaneous MCF-7/HER2-18 tumors with small-animal SPECT. However, ^{111}In -IGF-1(E3R) showed lower tumor uptake (2.5 %ID/g vs. 20.9 %ID/g) and lower tumor-to-liver ratios (0.09 vs. 7.5) than did ^{111}In -R1507 (39). Therefore, IGF-1R-expressing tumors are much better visualized with ^{111}In -

TABLE 1. Biodistribution of ^{111}In -R1507 and ^{89}Zr -R1507 in Mice with Subcutaneous SUM149 Xenografts at 7 Days After Injection

Tissue	^{111}In -R1507 (%ID/g)	^{89}Zr -R1507 (%ID/g)
Blood	5.6 ± 0.5	5.7 ± 0.7
Muscle	0.7 ± 0.1	0.7 ± 0.1
Tumor	20.9 ± 2.4	22.3 ± 2.5
Lung	4.5 ± 0.7	4.6 ± 0.5
Spleen	5.4 ± 0.9	5.7 ± 0.7
Kidney	4.4 ± 0.4	4.9 ± 0.7
Liver	2.9 ± 0.4	4.6 ± 0.4
Small intestine	2.5 ± 0.4	2.5 ± 0.4
Pancreas	1.0 ± 0.1	1.1 ± 0.1
Bone	1.3 ± 0.4	8.2 ± 4.2
Tumor-to-liver ratio	7.5 ± 1.2	4.8 ± 0.2
Tumor-to-blood ratio	3.8 ± 0.7	3.9 ± 0.5

Values are mean ± SD.

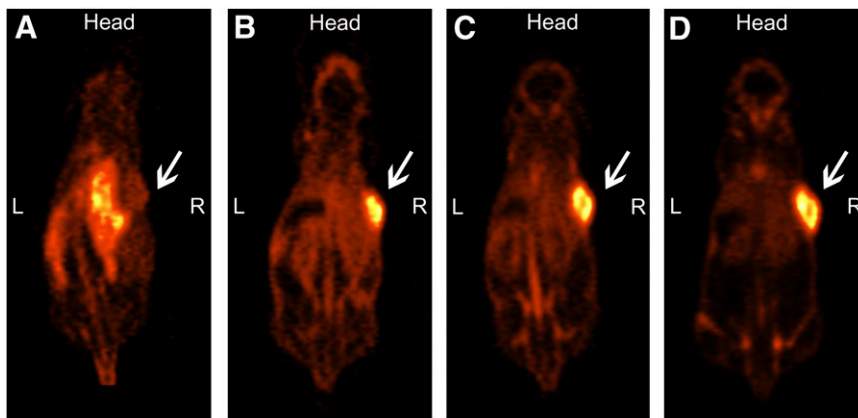


FIGURE 7. PET images of mouse with subcutaneous SUM149 tumor immediately after injection (A) and at 1 (B), 3 (C), and 7 (D) d after injection of 5 MBq of ^{89}Zr -R1507 (10 μg). Tumor-to-liver ratios in this mouse, calculated from PET images, were 1.8, 2.7, and 4.3 at 1, 3, and 7 d after injection, respectively. Ex vivo biodistribution study on day 7 revealed that tumor uptake of ^{89}Zr -R1507 for this mouse was 22 %ID/g. SUM149 tumors are indicated by arrows.

R1507 than with ^{111}In -IGF-1(E3R). Also small-molecule fluorophores have been used to image IGF-1R expression in MCF-7 tumors (40). In patients, however, fluorescent imaging cannot detect tumor lesions in deeper organs because of limited tissue penetrations of visible light.

CONCLUSION

Our experiments show that radiolabeled R1507 specifically accumulated in triple-negative SUM149 xenografts and that ^{111}In -R1507 SPECT and ^{89}Zr -R1507 PET can be used to visualize IGF-1R expression in vivo. In the future, these techniques may enable patient selection for IGF-1R-targeted therapy.

ACKNOWLEDGMENTS

We thank Melissa Roeffen, Bianca Lemmers-van de Weem, and Kitty Lemmens-Hermans for technical assistance. This study was financially supported by a personal research grant of the Dutch Research Council (016.096.010).

REFERENCES

- Carey LA, Dees EC, Sawyer L, et al. The triple negative paradox: primary tumor chemosensitivity of breast cancer subtypes. *Clin Cancer Res*. 2007;13:2329–2334.
- Dent R, Trudeau M, Pritchard KI, et al. Triple-negative breast cancer: clinical features and patterns of recurrence. *Clin Cancer Res*. 2007;13:4429–4434.
- Haffty BG, Yang Q, Reiss M, et al. Locoregional relapse and distant metastasis in conservatively managed triple negative early-stage breast cancer. *J Clin Oncol*. 2006;24:5652–5657.
- Rakha EA, El-Sayed ME, Green AR, Lee AH, Robertson JF, Ellis IO. Prognostic markers in triple-negative breast cancer. *Cancer*. 2007;109:25–32.
- Tischkowitz M, Brunet JS, Begin LR, et al. Use of immunohistochemical markers can refine prognosis in triple negative breast cancer. *BMC Cancer*. 2007;7:134.
- Bauer KR, Brown M, Cress RD, Parise CA, Caggiano V. Descriptive analysis of estrogen receptor (ER)-negative, progesterone receptor (PR)-negative, and HER2-negative invasive breast cancer, the so-called triple-negative phenotype: a population-based study from the California cancer Registry. *Cancer*. 2007;109:1721–1728.
- Harris LN, Broadwater G, Lin NU, et al. Molecular subtypes of breast cancer in relation to paclitaxel response and outcomes in women with metastatic disease: results from CALGB 9342. *Breast Cancer Res*. 2006;8:R66.
- Morris GJ, Naidu S, Topham AK, et al. Differences in breast carcinoma characteristics in newly diagnosed African-American and Caucasian patients: a single-institution compilation compared with the National Cancer Institute's Surveillance, Epidemiology, and End Results database. *Cancer*. 2007;110:876–884.
- Carey LA, Perou CM, Livasy CA, et al. Race, breast cancer subtypes, and survival in the Carolina Breast Cancer Study. *JAMA*. 2006;295:2492–2502.
- Irvin WJ Jr, Carey LA. What is triple-negative breast cancer? *Eur J Cancer*. 2008;44:2799–2805.
- Lerma E, Peiro G, Ramon T, et al. Immunohistochemical heterogeneity of breast carcinomas negative for estrogen receptors, progesterone receptors and Her2/neu (basal-like breast carcinomas). *Mod Pathol*. 2007;20:1200–1207.
- Feldser D, Agani F, Iyer NV, Pak B, Ferreira G, Semenza GL. Reciprocal positive regulation of hypoxia-inducible factor 1 α and insulin-like growth factor 2. *Cancer Res*. 1999;59:3915–3918.
- Hartog H, Wesseling J, Boezen HM, van der Graaf WT. The insulin-like growth factor 1 receptor in cancer: old focus, new future. *Eur J Cancer*. 2007;43:1895–1904.
- Samani AA, Yakar S, LeRoith D, Brodt P. The role of the IGF system in cancer growth and metastasis: overview and recent insights. *Endocr Rev*. 2007;28:20–47.
- Eckstein N, Servan K, Hildebrandt B, et al. Hyperactivation of the insulin-like growth factor receptor I signaling pathway is an essential event for cisplatin resistance of ovarian cancer cells. *Cancer Res*. 2009;69:2996–3003.
- Molloy CA, May FE, Westley BR. Insulin receptor substrate-1 expression is regulated by estrogen in the MCF-7 human breast cancer cell line. *J Biol Chem*. 2000;275:12565–12571.
- Dallas NA, Xia L, Fan F, et al. Chemoresistant colorectal cancer cells, the cancer stem cell phenotype, and increased sensitivity to insulin-like growth factor-I receptor inhibition. *Cancer Res*. 2009;69:1951–1957.
- Jones HE, Goddard L, Gee JM, et al. Insulin-like growth factor-I receptor signalling and acquired resistance to gefitinib (ZD1839; Iressa) in human breast and prostate cancer cells. *Endocr Relat Cancer*. 2004;11:793–814.
- Myers MG Jr, Grammer TC, Wang LM, et al. Insulin receptor substrate-1 mediates phosphatidylinositol 3'-kinase and p70S6k signaling during insulin, insulin-like growth factor-1, and interleukin-4 stimulation. *J Biol Chem*. 1994;269:28783–28789.
- He W, Craparo A, Zhu Y, et al. Interaction of insulin receptor substrate-2 (IRS-2) with the insulin and insulin-like growth factor I receptors: evidence for two distinct phosphotyrosine-dependent interaction domains within IRS-2. *J Biol Chem*. 1996;271:11641–11645.
- Giorgetti S, Pellicci PG, Pellicci G, Van OE. Involvement of Src-homology/collagen (SHC) proteins in signaling through the insulin receptor and the insulin-like-growth-factor-I-receptor. *Eur J Biochem*. 1994;223:195–202.
- Gualberto A, Pollak M. Emerging role of insulin-like growth factor receptor inhibitors in oncology: early clinical trial results and future directions. *Oncogene*. 2009;28:3009–3021.
- Zha J, O'Brien C, Savage H, et al. Molecular predictors of response to a humanized anti-insulin-like growth factor-I receptor monoclonal antibody in breast and colorectal cancer. *Mol Cancer Ther*. 2009;8:2110–2121.
- Cao L, Yu Y, Darko I, et al. Addiction to elevated insulin-like growth factor I receptor and initial modulation of the AKT pathway define the responsiveness of rhabdomyosarcoma to the targeting antibody. *Cancer Res*. 2008;68:8039–8048.
- Verel I, Visser GW, Boellaard R, Stigter-van WM, Snow GB, van Dongen GA. ^{89}Zr immuno-PET: comprehensive procedures for the production of ^{89}Zr -labeled monoclonal antibodies. *J Nucl Med*. 2003;44:1271–1281.
- Lindmo T, Boven E, Cuttitta F, Fedorko J, Bunn PA Jr. Determination of the immunoreactive fraction of radiolabeled monoclonal antibodies by linear extrapolation to binding at infinite antigen excess. *J Immunol Methods*. 1984;72:77–89.
- Koppe MJ, Hendriks T, Boerman OC, Oyen WJ, Bleichrodt RP. Radioimmunotherapy is an effective adjuvant treatment after cytoreductive surgery of experimental colonic peritoneal carcinomatosis. *J Nucl Med*. 2006;47:1867–1874.
- van der Have F, Vastenhouw B, Ramakers RM, et al. U-SPECT-II: an ultra-high-resolution device for molecular small-animal imaging. *J Nucl Med*. 2009;50:599–605.

29. Visser EP, Disselhorst JA, Brom M, et al. Spatial resolution and sensitivity of the Inveon small-animal PET scanner. *J Nucl Med.* 2009;50:139–147.
30. Brouwers AH, van Eerd JE, Frielink C, et al. Optimization of radioimmunotherapy of renal cell carcinoma: labeling of monoclonal antibody cG250 with ¹³¹I, ⁹⁰Y, ¹⁷⁷Lu, or ¹⁸⁶Re. *J Nucl Med.* 2004;45:327–337.
31. Press OW, Shan D, Howell-Clark J, et al. Comparative metabolism and retention of iodine-125, yttrium-90, and indium-111 radioimmunoconjugates by cancer cells. *Cancer Res.* 1996;56:2123–2129.
32. Dijkers EC, Kosterink JG, Rademaker AP, et al. Development and characterization of clinical-grade ⁸⁹Zr-trastuzumab for HER2/neu immunoPET imaging. *J Nucl Med.* 2009;50:974–981.
33. Perk LR, Visser GW, Vosjan MJ, et al. ⁸⁹Zr as a PET surrogate radioisotope for scouting biodistribution of the therapeutic radiometals ⁹⁰Y and ¹⁷⁷Lu in tumor-bearing nude mice after coupling to the internalizing antibody cetuximab. *J Nucl Med.* 2005;46:1898–1906.
34. Huang F, Greer A, Hurlburt W, et al. The mechanisms of differential sensitivity to an insulin-like growth factor-1 receptor inhibitor (BMS-536924) and rationale for combining with EGFR/HER2 inhibitors. *Cancer Res.* 2009;69:161–170.
35. Mukohara T, Shimada H, Ogasawara N, et al. Sensitivity of breast cancer cell lines to the novel insulin-like growth factor-1 receptor (IGF-1R) inhibitor NVP-AEW541 is dependent on the level of IRS-1 expression. *Cancer Lett.* 2009;282:14–24.
36. Karna E, Mityk W, Surazynski A, Palka JA. Protective effect of hyaluronic acid on interleukin-1-induced deregulation of beta1-integrin and insulin-like growth factor-I receptor signaling and collagen biosynthesis in cultured human chondrocytes. *Mol Cell Biochem.* 2008;308:57–64.
37. Massicotte F, Aubry I, Martel-Pelletier J, Pelletier JP, Fernandes J, Lajeunesse D. Abnormal insulin-like growth factor 1 signaling in human osteoarthritic subchondral bone osteoblasts. *Arthritis Res Ther.* 2006;8:R177.
38. Philippou A, Halapas A, Maridaki M, Koutsilieris M. Type I insulin-like growth factor receptor signaling in skeletal muscle regeneration and hypertrophy. *J Musculoskelet Neuronal Interact.* 2007;7:208–218.
39. Cornelissen B, McLarty K, Kersemans V, Reilly RM. The level of insulin growth factor-1 receptor expression is directly correlated with the tumor uptake of ¹¹¹In-IGF-1(E3R) in vivo and the clonogenic survival of breast cancer cells exposed in vitro to trastuzumab (Herceptin). *Nucl Med Biol.* 2008;35:645–653.
40. Zhang H, Zeng X, Li Q, Gaillard-Kelly M, Wagner CR, Yee D. Fluorescent tumour imaging of type I IGF receptor in vivo: comparison of antibody-conjugated quantum dots and small-molecule fluorophore. *Br J Cancer.* 2009;101:71–79.